UC Irvine
UC Irvine Previously Published Works

Title

Effect of high-resolution spatial soil moisture variability on simulated runoff response using a distributed hydrologic model

Permalink

https://escholarship.org/uc/item/0zv0s1jt

Journal

Hydrology and Earth System Sciences, 15(4)

ISSN

1607-7938

Authors

Minet, J.
Laloy, E.
Lambot, S.
et al.

Publication Date

2011-04-29

DOI

10.5194/hess-15-1323-2011

Peer reviewed

**Hydrology and
Earth System
Sciences**

Effect of high-resolution spatial soil moisture variability on simulated runoff response using a distributed hydrologic model

J. Minet[1]**, E. Laloy**[2]**, S. Lambot**[1,3]**, and M. Vanclooster**[1]

[1]Earth and Life Institute, Université catholique de Louvain, Croix du Sud 2 BP 2, 1348 Louvain-la-Neuve, Belgium
[2]Department of Civil and Environmental Engineering, University of California, Irvine, CA 92697-2175, USA
[3]Agrosphere (IBG-3), Institute of Bio- and Geosciences, Forschungszentrum Jülich GmbH, 52425 Jülich, Germany

Abstract. The importance of spatial variability of antecedent soil moisture conditions on runoff response is widely acknowledged in hillslope hydrology. Using a distributed hydrologic model, this paper aims at investigating the effects of soil moisture spatial variability on runoff in various field conditions and at finding the structure of the soil moisture pattern that approaches the measured soil moisture pattern in terms of field scale runoff. High spatial resolution soil moisture was surveyed in ten different field campaigns using a proximal ground penetrating radar (GPR) mounted on a mobile platform. Based on these soil moisture measurements, seven scenarios of spatial structures of antecedent soil moisture were used and linked with a field scale distributed hydrological model to simulate field scale runoff. Accounting for spatial variability of soil moisture resulted in general in higher predicted field scale runoff as compared to the case where soil moisture was kept constant. The ranges of possible hydrographs were delineated by extreme scenarios where soil moisture was directly and inversely modelled according to the topographic wetness index (TWI). These behaviours could be explained by the sizes and locations of runoff contributing areas, knowing that runoff was generated by infiltration excess over a certain soil moisture threshold. The most efficient scenario for modelling the within field spatial structure of soil moisture appeared to be when soil moisture is directly arranged according to the TWI, especially when measured soil moisture and TWI were correlated. The novelty of this work is to benefit from a large set of high-resolution

soil moisture measurements allowing to model effectively the within field distribution of soil moisture and its impact on the field scale hydrograph. These observations contributed to the current knowledge of the impact of antecedent soil moisture spatial variability on field scale runoff.

1 Introduction

The antecedent soil moisture condition prior to rainfall is a key factor in determining the hydrological response as it mainly governs the generation of runoff due to its effect on infiltration capacities. In hydrologic modelling, the prediction of runoff is therefore highly sensitive to the description of antecedent soil moisture conditions. The response of the hydrologic models to antecedent soil moisture is moreover often highly non-linear and shows a threshold behaviour (Zehe and Blöschl, 2004).

The effect of antecedent soil moisture spatial variability on hydrologic response at the field scale has been widely addressed in numerous studies through hydrologic modelling. The large effect of soil moisture variability on runoff response is to be attributed to the prominent role of soil moisture in runoff generation by either infiltration excess or saturation excess overland flows (Zehe and Blöschl, 2004). The location of runoff contributing areas, which are directly related to the soil moisture state, modulates the hydrologic response as generated runoff can re-infiltrate on its way downhill to the catchment outlet. In particular, Merz and Plate (1997); Merz and Bardossy (1998) and Bronstert and Bardossy (1999) showed that accounting for the spatial variability of antecedent soil moisture yields a greater runoff

compared to assuming uniform soil moisture conditions, denoting the non-linear response of the hydrologic model to antecedent moisture conditions. Regarding the type of variability, Merz and Plate (1997); Merz and Bardossy (1998) and Zehe et al. (2005) observed that a structured soil moisture pattern results in a greater runoff than a stochastic random variability, especially when large contributing areas were connected by a flow channel to the outlet. In contrast to this, Bronstert and Bardossy (1999) observed the smallest runoff response with structured soil moisture patterns compared to random patterns. This was attributed to the actual poor organisation of the structured pattern that was observed in dry conditions. Bronstert and Bardossy (1999) also showed that the introduction of topographic data in modelling of soil moisture was the best strategy to obtain a runoff response close to the measured outlet response. The importance of spatial variability of soil moisture for hydrologic modelling has also received a specific attention in data assimilation studies (Houser et al., 1998; Pauwels et al., 2001; Crow and Ryu, 2009; Brocca et al., 2010).

The way spatial variability of soil moisture impacts runoff is depending on model parameterisation, average soil moisture state itself (Zehe et al., 2005, 2010) and type of rainfall which is considered (Bronstert and Bardossy, 1999; Noto et al., 2008). In particular, Noto et al. (2008) pointed out that the well-known high sensitivity of the hydrologic model to antecedent soil moisture conditions may be observed only under specific rainfall forcing. In that respect, in a semi-arid catchment, Castillo et al. (2003) noticed that runoff response is insensitive to antecedent soil moisture conditions for high intensity rainfalls or for poorly permeable soils. Hence, in some conditions, assuming a constant mean soil moisture may be sufficient to correctly model the rainfall-runoff response, particularly if extreme events are considered (e.g., in flood risks applications). The effect of spatial variability of soil moisture were particularly observed in steep topography (Kuo et al., 1999; Castillo et al., 2003) that allows lateral redistribution of water over the catchment. It is also expected to be substantial in dry conditions as shown in Merz and Plate (1997) where two antecedent soil moisture conditions were compared. It is worth noting that highly wet conditions inherently exhibit low spatial variability because of the bounded behaviour of soil moisture by saturation (Famiglietti et al., 2008).

The scale aggregation of soil moisture data as well as other inputs (e.g., digital elevation model) can also highly alter the accuracy of the response of the hydrologic model. Using information theory, Kuo et al. (1999) noticed that the deviations in simulated runoff increase proportionally with the grid size of a distributed hydrologic model, especially for steep topography and in wet conditions. Finally, the high sensitivity of runoff response to antecedent soil moisture implies that uncertainty in soil moisture characterisation exerts a large effect on the predictability of hydrologic models, similarly to the effect of soil moisture variability (Zehe

and Blöschl, 2004). Still, the effect of the variability of soil moisture on runoff response has to be investigated for various conditions of catchment attributes, soil moisture patterns and rainfall forcing.

In the near future, the availability of in-situ measurements of soil moisture for hydrologic applications is expected to greatly increase through the development of soil moisture dedicated remote sensing platforms (Wagner et al., 2007), soil moisture electrical sensors and their implementation in sensor networks (Vereecken et al., 2008; Robinson et al., 2008) and non-invasive sensors such as ground penetrating radar (GPR) (Huisman et al., 2003; Lambot et al., 2008a). In that respect, GPR has shown great potential to accurately characterise soil moisture at the field scale with high resolution (Serbin and Or, 2005; Weihermüller et al., 2007; Lambot et al., 2008b; Minet et al., 2011). As pointed out by Western et al. (1999), high-resolution soil moisture datasets are required to readily assess the effect of antecedent soil moisture conditions, rather than relying on few point values that may not capture the real soil moisture patterns. Nevertheless, hydrologic modelling of processes occurring at an intermediate scale between coarse-scale ($\sim$km) remote sensing and fine-scale ($\sim$m) soil moisture measurement techniques is limited by a scale-gap in soil moisture information. The combination of these two types of information by disaggregating (or downscaling) coarse-scale to fine-scale soil moisture data is thus of particular interest (Crow et al., 2000). In that respect, Loew and Mauser (2008) investigated the use of prior information on spatially persistent soil moisture patterns to disaggregate coarse-scale remotely-sensed soil moisture data. Disaggregated soil moisture values may be also particularly valuable for soil moisture data assimilation in hydrologic models (Merlin et al., 2006).

To extent previous work about the strong nonlinear effect of antecedent soil moisture on field scale hydrological response in temperate climate conditions, this paper aims to: (1) investigate the effect of different scenarios of high-resolution spatial structure of antecedent soil moisture on simulated runoff at the field scale and; (2) find the spatial structure of the within field soil moisture that most closely approaches the measured soil moisture pattern in terms of hydrologic response. Seven scenarios of antecedent soil moisture patterns, together with GPR measured soil moisture patterns, were defined in order to determine which degree of description of soil moisture spatial variability is necessary to get an adequate estimation of the runoff. The main novelties of this work compared to the previous studies are: (1) to benefit from a fast soil moisture mapping technique at high resolution ($\sim$m) at the field scale (several ha) and; (2) to rely on ten field acquisitions of soil moisture in different field and moisture conditions. This work may also help when coarse-scale remotely-sensed soil moisture data are to be disaggregated into fine-scale patterns in hydrologic or climatic models.

Table 1. Description of the agricultural fields and resolutions used in hydrologic simulations.

Field	Location		Area [ha]	Elevation range [m]	Resolution [m]	Soil type	Land cover
Burnia	4°38′33″ E	50°40′10″ N	2.29	14	7	silt loam	wheat
Marbaix	4°38′40″ E	50°40′07″ N	5.73	14	10	silt loam	wheat
Walhain	4°41′32″ E	50°36′11″ N	5.14	16	15	silt loam	barley
Keispelt	6°04′57″ E	49°41′33″ N	3.29	18	12.5	sandy loam	wheat
Walsdorf	6°09′19″ E	49°55′45″ N	2.39	12	10	shaly silt loam	bare

2 Materials and methods

2.1 Agricultural fields

In this paper, we used soil moisture data collected during ten GPR acquisitions performed in five different agricultural fields situated in the centre of Belgium and Luxembourg (see Table 1). The fields are characterized by relatively similar topography, soil type and land cover but the acquisitions were performed in different moisture conditions. The first three fields, that are called, Burnia, Marbaix and Walhain, pertain to the loess belt area in Belgium and are characterised by a flat topography and a silt loam soil. According to the national Belgian soil database (Van Orshoven and Vandenbroucke, 1993) and following a profile matching technique, the texture of this soil consists of 4 % of sand, 82 % of silt and 14 % of clay for the Burnia and Marbaix soil and 4 % of sand, 79 % of silt and 17 % of clay for the Walhain soil. The last two fields, that are located in Luxembourg and called Keispelt and Walsdorf, are characterised by a gentle topography. They are classified as sandy loam and shaly silt loam soils, respectively.

The GPR acquisitions were performed in spring when fields were covered by barley or wheat, except for the Walsdorf site where acquisition was performed in summer after barley cropping. All the acquisitions were performed on bare or nearly-bare soils with vegetation height less than 10 cm and a soil roughness less than 5 cm, thus avoiding scattering issues in the measured GPR data. In each field surveyed by the GPR, the largest catchment was delineated, as some fields are actually constituted of several catchments. Moreover, the fields were considered as hydrologically isolated from the neighbouring plots (i.e., by ditches or rural roads along the field limits). For some fields, that were, Keispelt, Marbaix and Burnia, the delineated catchments encompasses the whole surveyed field. Catchment areas are given in Table 1.

2.2 Sensing of soil moisture by ground penetrating radar

In this paper, soil moisture was measured by a proximal off-ground GPR system operating in the frequency domain (200–2000 MHz) (Lambot et al., 2004, 2006). For non-magnetic soils, the GPR wave propagation is governed by the soil dielectric permittivity ε and electrical conductivity σ. As the dielectric permittivity of water ($\varepsilon_{\mathrm{w}} \approx 80$) is much larger than the one of the soil particles ($\varepsilon_{\mathrm{s}} \approx 5$) and air ($\varepsilon_{\mathrm{a}} = 1$), GPR measurements are mainly influenced by the soil water content. Soil moisture was derived from the measured GPR data using inversion of the GPR data after soil-antenna interactions filtering (Lambot et al., 2004). The surface soil relative dielectric permittivity was retrieved by inverting the GPR data focused on the surface reflection using an electromagnetic model simulating the propagation of the wave into the soil (Lambot et al., 2006). In order to avoid noise in the GPR data that arises at high frequencies because of soil roughness, the inversions were led in the limited frequency range from 200 to 800 MHz. Optimisation was performed using a local search algorithm, that was, the Levenberg-Marquardt algorithm (Marquardt, 1963). Two parameters were optimised in the inversion, that were, the surface soil dielectric permittivity ε and the GPR antenna height above the ground. In this paper, the soil electrical conductivity σ was not optimised but was directly derived from the soil moisture θ using a laboratory-calibrated relationship following the model of Rhoades et al. (1976):

$$\sigma = (a\theta^2 + b\theta)\sigma_{\mathrm{w}} + \sigma_{\mathrm{s}} \tag{1}$$

where the parameters are set to $a = 1.85$, $b = 3.85 \times 10^{-2}$, $\sigma_{\mathrm{w}} = 0.075\,\mathrm{Sm}^{-1}$ and $\sigma_{\mathrm{s}} = 5.89 \times 10^{-4}\,\mathrm{Sm}^{-1}$.

After GPR inversion, the optimised surface soil dielectric permittivity ε was translated into surface soil moisture θ using the Topp's petrophysical relationship (Topp et al., 1980):

$$\theta = -5.3 \times 10^{-2} + 2.92 \times 10^{-2}\varepsilon - 5.5 \times 10^{-4}\varepsilon^2 + 4.3 \times 10^{-6}\varepsilon^3 \tag{2}$$

The GPR method for soil moisture retrieval was widely validated in laboratory conditions (Lambot et al., 2004, 2006; Minet et al., 2010) and applied to field conditions (Weihermüller et al., 2007; Lambot et al., 2008b; Jadoon et al., 2010; Minet et al., 2011). The GPR-derived soil moisture uncertainty was quantified in Jadoon et al. (2010) and a RMSE of 0.025 in terms of volumetric water content between TDR and GPR estimates was found.

The GPR-derived soil moisture reflects the surface soil moisture with a depth of investigation of about 5–10 cm. This relatively shallow characterisation of soil moisture may be a limitation for using the soil moisture data in a hydrologic

Table 2. GPR soil moisture ($[m^3\,m^{-3}]$) acquisitions. The number of measured points, the duration of the acquisition, the mean (μ_θ) and standard deviation (σ_θ) of soil moisture, variogram parameters (Nugget effect $[m^3\,m^{-3}]^2$, Sill $[m^3\,m^{-3}]^2$ and Range $[m]$), the ratio between the nugget effect and the sill (Nug./Sill) and the coefficient of correlation between the TWI and soil moisture ($r_{\mathrm{TWI},\theta}$) are presented.

		N° of points	Duration	μ_θ	σ_θ	Nug. effect	Sill	Range	Nug./Sill [%]	$r_{\mathrm{TWI},\theta}$
Walhain	07/04/2008	1008	4h56'	0.301	0.060	0.0006	0.0028	35	20	−0.064
Keispelt	13/03/2009	1311	48'	0.262	0.106	0.0033	0.0076	112	43	0.156
Marbaix	19/03/2009	3786	1h51'	0.106	0.051	0.0008	0.0023	177	33	0.170
Marbaix	15/04/2009	2911	2h02'	0.115	0.047	0.0006	0.0027	260	23	0.385
Walsdorf	21/07/2009	3248	1h08'	0.173	0.071	0.0019	0.0038	21	50	−0.235
Burnia	15/03/2010	1496	1h09'	0.226	0.067	0.0013	0.0041	79	32	0.139
Burnia	18/03/2010	1252	56'	0.234	0.062	0.0016	0.0034	77	47	0.011
Burnia	24/03/2010	1429	1h01'	0.238	0.063	0.0014	0.0036	70	39	−0.050
Burnia	30/03/2010	1227	1h32'	0.304	0.154	0.0065	0.0248	120	26	0.062
Burnia	06/04/2010	1759	51'	0.309	0.155	0.0064	0.0258	175	25	0.120

model, as the hydrological active soil layer extends up to 20 cm in the hydrologic model and because of the possible decoupling of surface and subsurface soil moisture (Capehart and Carlson, 1997; Vereecken et al., 2008). Nevertheless, the use of a proximal GPR operating in a large frequency bandwidth and at relatively low frequencies inherently provides a deeper characterisation of soil moisture than remote sensing instruments. Moreover, a deeper characterisation could be obtained using a multi-layered soil model, as shown in Minet et al. (2011). In this study, it is assumed that the surface soil moisture reflects the soil moisture of the hydrological active soil layer or, at least, its spatial variability.

For field acquisition, the GPR system was mounted on an all-terrain vehicle (ATV) with a differential global positioning system (DGPS) and a PC (Minet et al., 2011). Real-time GPR measurements were performed at a regular distance spacing of two meters in the same track, according to the DGPS position, which is known with a precision of about 3 cm. The ATV followed parallel tracks with a distance spacing of 5 to 15 m between tracks. More than 1000 points were measured per hour, with a driving speed of about $5\,\mathrm{km\,h^{-1}}$. The antenna footprint where soil moisture is measured has a diameter of about 1.5 m. The proximity of the support and resolution scales permits to acquire nearly continuous soil moisture patterns similarly to radar remote sensing platforms but at higher resolution. Table 2 summarises the 10 GPR acquisitions and shows the number of measurement points and the duration of the acquisition for each field campaign. Time-lapse measurements were performed in two fields only, i.e., in Marbaix and Burnia, in spring 2009 and 2010, respectively. These time-lapse acquisitions permitted to compare the effect of different moisture conditions only.

2.3 Antecedent soil moisture scenarios

Soil moisture spatial variability can be analysed in terms of stochastic or deterministic variability (Blöschl and Siva-

palan, 1995). Stochastic variability (or random, non-structured variability) of soil moisture entails that soil moisture can not be a completely deterministic variable based on local attributes but rather a variable with global statistical properties that can be determined. On the other hand, soil moisture can be viewed as a spatially deterministic (or structured) variable that is uniquely determined by spatial conditions, mainly topography, soil properties, and vegetation cover. The introduction of auxiliary spatial data (e.g., topography) to simulate soil moisture thus results in deterministic soil moisture patterns. Between these two extremes, hydrological systems exhibit soil moisture conditions that can be modelled from pure random variability to highly structured soil moisture patterns, with intermediate degree of organisation (Western et al., 1999). It is worth mentioning that a stochastic soil moisture description implies several random realisations while a deterministic soil moisture pattern is usually a unique realisation. Except the pure random case, soil moisture patterns can be captured using variograms or connectivity functions.

In this study, soil moisture scenarios are based on point measured data, that are displayed as an example for Marbaix, 15 April 2009 in Fig. 1. In order to assess the effect of different antecedent soil moisture conditions in hydrologic modelling, seven different types of antecedent soil moisture maps were constructed (see further explanations in this section below):

1. *Reference*: GPR-derived measured values, $\theta = \theta_{\mathrm{GPR}}$;

2. *Constant*: $\theta = \theta_{\mathrm{mean}} = \mathrm{constant}$;

3. *Structured*: Measured values sorted according to the TWI;

4. *Structured*$_{\mathrm{inv}}$: Measured values inversely sorted according to the TWI;

5. *Random*: Randomly permutated values;
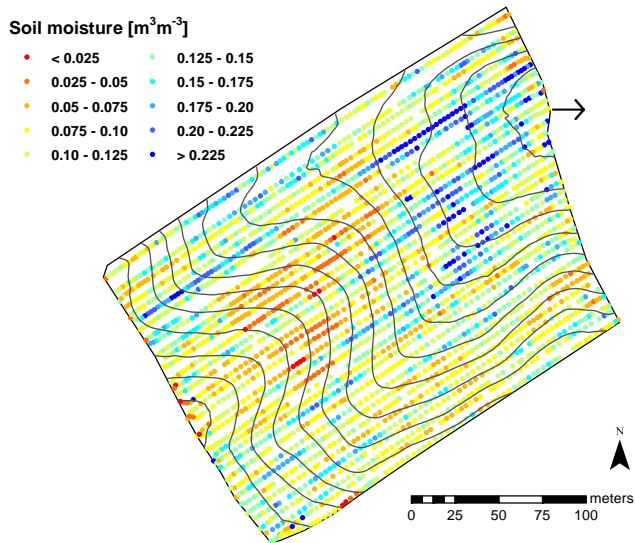
Fig. 1. Maps of soil moisture point-values retrieved by GPR inversions from the field acquisition in Marbaix, 15 April 2009. Contour lines with an interdistance of one meter are depicted in black lines. The outlet of the field is indicated by the black arrow. Projected coordinate system: Belgian Lambert 1972.

6. *Variogram*: Spatially coherent values using a variogram;

7. *Connected*: Spatially coherent and connected values.

Scenarios 2 to 4 are deterministic scenarios, i.e., they consist of a unique realisation, while scenarios 5 to 7 are stochastic scenarios, for which 1000 realisations were produced. These soil moisture scenarios are all based on GPR-derived soil moisture that was measured during field acquisitions. Figure 2 presents all soil moisture scenarios (except the *Constant*) for the field of Marbaix, 15 April 2009.

The soil moisture values measured by the GPR were not regularly spaced in the field, but rather followed the acquisition tracks (see Fig. 1). The hydrologic model however requires as an input perfectly grid-shaped antecedent soil moisture maps. Therefore, the measured values must be rasterised. The first scenario (*Reference*, Fig. 2a), that is based on the real locations of GPR measured values, was thus made by filling a regular grid with the average of the measured values that fell into each pixel of the grid. The resolutions of the grids (see Table 1) were set as the maximum resolution that avoids having an empty pixel in the grid.

For the second scenario (*Constant*), soil moisture values were set as constant over space and equal to the mean of the measured values from the first map. This map is not presented in Fig. 2.

In the third scenario (*Structured*, Fig. 2b), measured values were sorted according to the topographic wetness index
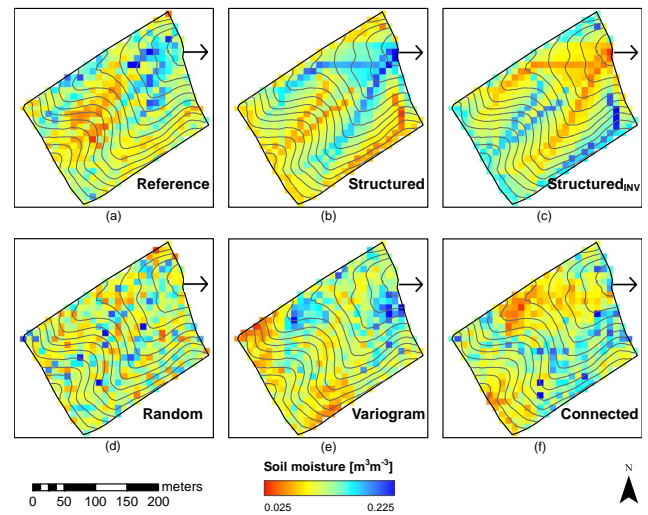
Fig. 2. Antecedent soil moisture maps for Marbaix, 15 April 2009, used as an input in the hydrologic model with measured grided values **(a)**, measured values rearranged according the TWI **(b)**, measured values inversely rearranged according the TWI **(c)**, randomly permuted values **(d)**, simulated values using a variogram **(e)** and connected simulated values **(f)**. The outlet location and direction are indicated with an arrow.

(TWI), as defined by Beven and Kirkby (1979):

$$\text{TWI} = \ln\left(\frac{a}{\tan(\beta)}\right) \qquad (3)$$

where a is the raster of the flow accumulation and β is the raster of the slope expressed in %. We used a single direction algorithm to compute the flow accumulation raster, as was used in previous studies (e.g., Merz and Plate, 1997). The TWI was preliminary computed over the fields using a digital elevation model of same resolution that was set in the first scenario. Then, moisture and TWI values were ranked and moisture values were attributed to the pixels where the TWI was in the same rank. The fourth scenario (*Structured*$_{\text{inv}}$, Fig. 2c) is the counterpart of the third one, that is, soil moisture and TWI values were inversely ranked, so that the pixels with the highest TWI values received the lowest soil moisture values.

The TWI was chosen for modelling structured soil moisture patterns because of the lack of other detailed sources of information for these fields (e.g., soil properties, vegetation) and for its high predictive power in wet conditions (Western et al., 1999). The limited elevation range of the fields may however limit the redistribution of water according to the topography and restrain the explanatory power of the TWI for soil moisture in these fields. Although high-resolution soil information at the field scale could have provided more insights for explaining moisture patterns, no high-resolution soil parameters can be usually found at the catchment scale (>10 km). We thus investigated the use of topographically-derived indices (i.e., TWI) for soil moisture modelling in a

data-scarcity context. As soils were bare or nearly-bare, the influence of vegetation heterogeneities on spatial soil moisture variability might be furthermore limited in our study. In addition, land cover heterogeneities are limited in our study as the fields are managed as single plots. For larger catchment scale (>10 km), land cover differences among the fields may better explain soil moisture patterns (Western et al., 1999). For drier climatic conditions, when potential evapotranspiration exceeds precipitation, local controls as potential radiative indices have shown better correlations with observed soil moisture (Grayson et al., 1997). Some reviews about the predictive power of the TWI for soil moisture can be found in Western et al. (1999) and Sørensen et al. (2006).

The fifth scenario (*Random*, Fig. 2d) maps were made by randomly permuting the measured values over space. As the random process can lead to different maps, 1000 realisations of this scenario were repeated, as well as for the two following scenarios (stochastic variability scenarios).

The sixth scenario (*Variogram*, Fig. 2e) maps were made by simulating gaussian soil moisture patterns using variograms describing the spatial dependence of soil moisture. Variograms were computed considering the spatial dependence of the data along the acquisition lines only, neglecting the spatial dependence of the data of adjacent lines (Minet et al., 2011). An exponential model accounting for a nugget effect was fitted for all the variograms. Zero-mean gaussian distributed values were then simulated in each grid pixel using an implementation of the sequential non conditional method. Finally, measured values were ranked and attributed to the pixels where the simulated values were in the same rank. This ranking procedure permitted therefore to preserve exactly the same distribution of values as in the *Reference*, *Random*, *Structured* and *Structured*$_\mathrm{inv}$ scenarios.

The seventh scenario (*Connected*, Fig. 2f) is characterised by connected patterns of high soil moisture values. It was made following the method of Zinn and Harvey (2003) that was used here to produce a highly connected pattern of a given variable. First, spatially coherent values of a zero-mean gaussian distribution were simulated over the field extent as for the *Variogram* scenario. Second, the absolute value of the simulated values were taken, so that the locations where the values were close to zero (i.e., now the lowest values) became connected between them. In order to conserve the spatial properties of the simulated values after taking the absolute value, the parameters of the variogram must be initially modified. Hence, the range was multiplied by the scale factor of 1.86 and the nugget effect was divided by 2. Finally, inversely ranked measured values were attributed to the pixels where simulated values were in the same rank, so that the connected paths (i.e., the lowest simulated values) received the highest soil moisture values.

It is worth noting that all scenarios have the same mean as the *Reference* scenario, and that all scenarios, except the *Constant* one, show exactly the same soil moisture distribution as the *Reference* scenario, owing to the ranking proce-

dure. Moreover, the *Reference*, *Variogram* and *Connected* maps were characterised by the same variogram. This allowed to truly compare the modelling discharge between the scenarios. Actually, the *Random* scenario can yield exactly the same antecedent soil moisture maps that were realised with the *Reference*, *Structured*, *Structured*$_\mathrm{inv}$, *Variogram* and *Connected* scenarios, as the same values were merely rearranged according to different schemes. But the probability that the *Random* scenario yield a particular realisation is drastically low, i.e., equals to $\frac{1}{n!}$, where n is the number of grid cells per field, and may not be encountered in our study. The number of 1000 realisations for the stochastic scenarios is thus a tradeoff between the computation time and the desirable variability among realisations.

The hydrograph modelled with the *Reference* soil moisture map was assumed to be the reference hydrograph, as no measured discharges were available. Comparison of soil moisture scenarios were performed based on Nash-Sutcliffe efficiency (NSE) coefficients between the hydrographs simulated with the measured soil moisture pattern (*Reference* scenario) and the other scenarios.

The effect of soil moisture spatial variability may also depend on the resolution (grid size) of the distributed hydrologic model. For investigating scale aggregation of antecedent soil moisture maps, hydrologic simulations were also performed with increasing grid sizes for the field campaign of Marbaix, 19 April 2009 for the seven scenarios. Nine grid sizes, uniformly ranging from 10 to 30 m, were selected. The field campaign of Marbaix, 19 April 2009 was chosen as it was performed in the largest field at high resolution, maximising the grid size range.

2.4 Hydrologic model

In this work, we used the hydrological component of the continuous runoff and erosion CREHDYS model (see Laloy and Bielders (2008, 2009) for a comprehensive model description). It can be used at rainfall event scale to simulate high-frequency variability in rainfall-runoff processes. Short time steps are then required to properly capture soil physical dynamics. Consequently, the model requires one minute time step rainfall data as input. The model is spatially distributed and the flow path must be derived from topography through a flow accumulation grid. As we used the model for event-scale simulations only, the relevant modelled processes for runoff prediction are infiltration, soil depressional storage filling and runoff flow. For simplicity, no surface storage was however considered in this study. Infiltration is computed using the Green-Ampt model (Green and Ampt, 1911) which assumes a uniform wetting front infiltrating vertically. A single soil layer is assumed, which results in a single effective hydraulic conductivity along the entire topsoil depth. In its current form, the CREDHYS model therefore simulates infiltration-excess overland flow only and does not simulate saturation-excess runoff caused by shallow impervious layer

or perched aquifers. Runoff flow is routed along flow paths using a one-dimensional kinematic wave equation. Although not strictly required by the model to simulate the runoff dynamics at the event scale, note that percolation is computed within and between precipitations using the method of Savabi and Williams (1995). In addition, no evapotranspiration is taken into account within a single rainfall event.

The same rainfall forcing was used for every simulation. It was recorded in central Belgium and corresponds to a short and intensive storm with a return period of 6 yr (17.4 mm in 16 min). Because no discharge measurements are available, the hydrologic model could not be specifically calibrated for each of the fields. We therefore selected a typical model parameterisation for a mildly crusted bare loamy soil. In the absence of surface storage, the soil properties to be considered by the model are the effective saturated soil hydraulic conductivity, KS [$\mathrm{mm\,h^{-1}}$], the absolute value of the Green-Ampt soil matrix potential at the wetting front, ψ [mm], the antecedent soil moisture, θ [$\mathrm{m^3\,m^{-3}}$], the volumetric soil moisture content at saturation, θ_{SAT} [$\mathrm{m^3\,m^{-3}}$], the control depth for computing water balance, DF [m], the Manning's n friction coefficient [$\mathrm{m^{-1/3}\,s}$] and the percolation submodel parameters (see Laloy and Bielders (2008) for details). Based on the values found in Laloy and Bielders (2008); Laloy et al. (2010), we fixed KS at $25\,\mathrm{mm\,h^{-1}}$ (Burnia site) and $20\,\mathrm{mm\,h^{-1}}$ (other fields), ψ to 100 mm, θ_{SAT} to $0.50\,\mathrm{m^3\,m^{-3}}$, DF to 0.2 m, and n to $0.03\,\mathrm{m^{-1/3}\,s}$. Those values were used for all field simulations. The KS parameter was set at a slightly higher value for the Burnia site in order to generate runoff responses suitable for a meaningful comparison among fields and antecedent soil moisture scenarios. The KS equal to $20\,\mathrm{mm\,h^{-1}}$ was too small for Burnia site for generating differences between scenarios. The KS parameters were thus set accordingly the range of values found in Laloy and Bielders (2008) and Laloy et al. (2010) for a similar soil and for observing different runoff responses according to soil moisture scenarios. Lastly, it is worth mentioning that antecedent soil moisture θ was found to be one of the most sensitive parameters of CREHDYS with respect to runoff production (Laloy and Bielders, 2008). Hence, as the model is spatially-distributed, it is expected that spatial organisation of soil moisture strongly affects the runoff prediction at the outlet.

3 Results

3.1 Soil moisture data measured by ground penetrating radar

Table 2 presents the within-field mean and standard deviation of GPR measured soil moisture and the parameters of the fitted variograms for the ten field campaigns. As an example, Fig. 1 shows the map of surface soil moisture measured by GPR in Marbaix on the 15 April 2009. It is worth noting
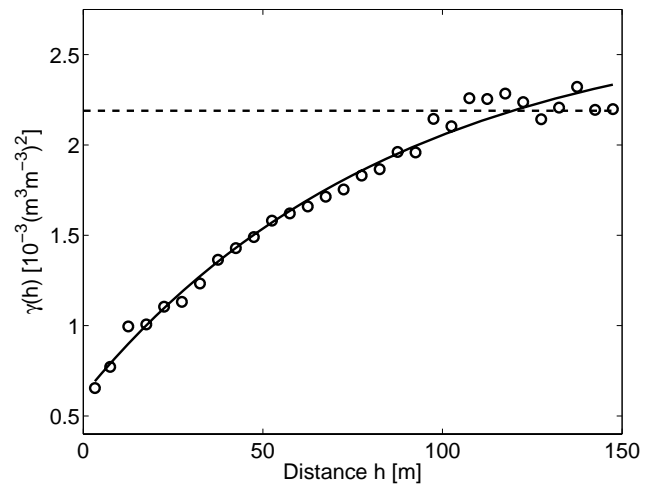

Fig. 3. Variogram of soil moisture computed for the field campaign in Marbaix, 15 April 2009 with a class distance from 0 to 150 m by a step of 5 m. A variogram using an exponential model is fitted on the data. The total variance of soil moisture is depicted with the dashed line.

that the point-symbols appear around two times larger on the map compared to the real GPR antenna footprint size. Soil moisture conditions were clearly dry for this GPR acquisition, with a corresponding smaller variability compared to the other acquisitions (see Table 2).

Soil moisture values appeared globally spatially coherent, although some nugget effect can be observed between neighbouring points. In particular, we could notice a line effect with a high spatial coherence for points along the same acquisition line (i.e., the acquisition tracks), whereas there were some abrupt changes when moving to adjacent lines, as already observed and discussed in Minet et al. (2011). At a larger scale however, soil moisture patterns were mainly related to the topography, that is, hilltops were drier than the thalwegs. The wettest areas appeared in the bottom of the thalwegs and near the outlet.

Figure 3 shows the variogram of soil moisture values computed along the acquisition lines for the field campaign in Marbaix, 15 April 2009. Spatial coherence was observed, with a regular increase of soil moisture variance with increasing distance classes up to the range, which reached 260 m, while other field campaigns showed smaller ranges. The nugget effect accounted for 23% of the total sill (Table 2). Pearson's coefficients of correlation between the TWI and measured soil moisture from the *Reference* maps were computed ($r_{\mathrm{TWI},\theta}$, Table 2, last column) and was equal to 0.385 for Marbaix, 15 April 2009. For the other field campaigns, the correlation between the TWI and soil moisture was always lower and even negative, as for, e.g., Walsdorf.
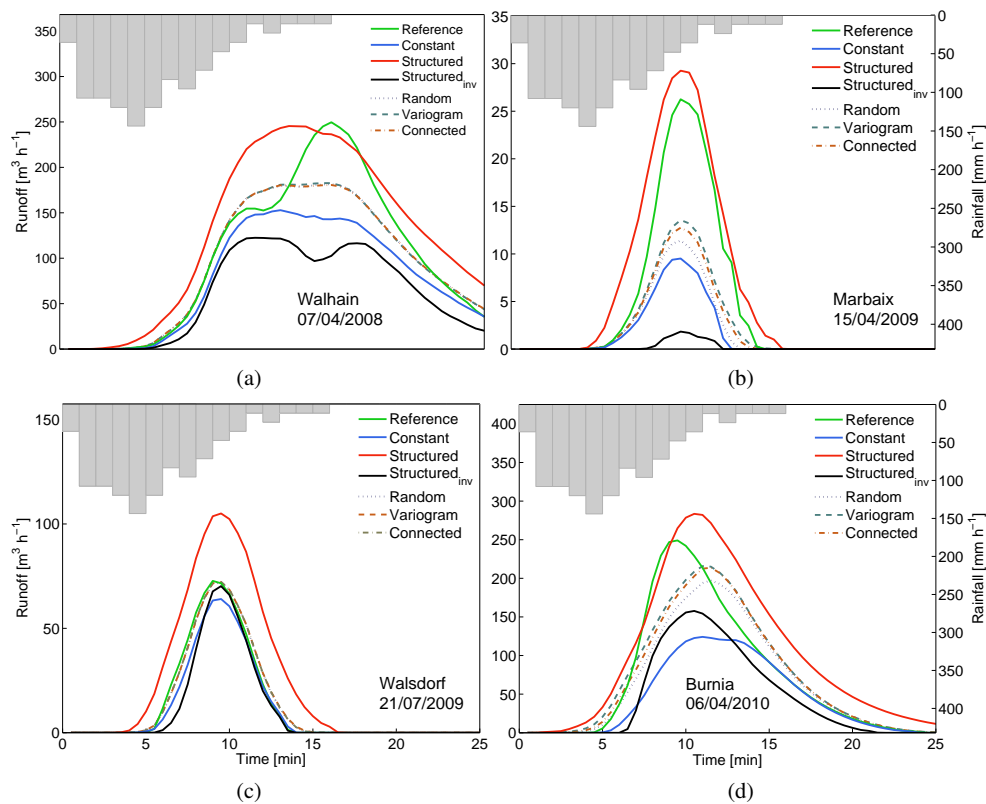
Fig. 4. Hydrographs from hydrologic simulations using the antecedent soil moisture maps from all scenarios for 4 field campaigns: Walhain – 07/04/2008 **(a)**, Marbaix – 15/04/2009 **(b)**, Walsdorf – 21/07/2009 **(c)** and Burnia – 06/04/2010 **(d)**. For stochastic soil moisture scenarios, i.e., *Random*, *Variogram*, *Connected*, the average hydrographs on the 1000 realisations are depicted. The rainfall is depicted by the bars of the second y-axis.

3.2 Effect of antecedent soil moisture on hydrographs

3.2.1 Hydrographs simulated with the deterministic soil moisture maps

Table 3 presents the runoff peaks and total runoff volumes resulting from the hydrologic simulations for the ten field campaigns and the seven scenarios. Figure 4 shows the hydrographs for four field campaigns only. For stochastic soil moisture scenarios, i.e., *Random*, *Variogram*, *Connected*, the average hydrographs of the 1000 realisations are depicted.

The *Constant* scenario, where soil moisture uniformly equals the mean value, showed a lower runoff peak and volume compared to all other scenarios, except the *Structured*$_{inv}$. For Burnia, 30/03/2010 and 06/04/2010, the smallest runoff peaks were found with the *Constant* scenario. The hydrographs simulated with the *Structured* and *Structured*$_{inv}$ scenarios completely delineated the range of variation of the other hydrographs for Marbaix – 15/04/2009 (Fig. 4b) as well as for Marbaix – 19/03/2009 and for the first three dates in Burnia. For the other field campaigns, although some scenarios (e.g., the *Reference*) can exceed this range, the hydrographs from the two soil moisture maps based on the TWI

(i.e., *Structured* and *Structured*$_{inv}$) generally gave the range of variation for the other hydrographs. In terms of runoff volume, the *Structured* scenario always resulted in the largest discharge. The *Structured*$_{inv}$ scenario resulted in the lowest runoff volume in 9 out of 10 field campaigns. It is worth noting that large differences in runoff peak and volumes existed between the different dates of the time-lapse acquisitions in Burnia and Marbaix. The amount of runoff appeared to be largely sensitive to the wetness state of the antecedent conditions.

As mean soil moisture increases, the range of variation of the hydrographs between the two extreme scenarios (*Structured* and *Structured*$_{inv}$) tends however to diminish. Figure 5 shows the relative difference between *Structured* and *Structured*$_{inv}$ runoff volume as a function of the mean soil moisture in the field. There was a good agreement between these two variables considering the Belgian fields (Burnia, Marbaix, Walhain) only, with a coefficient of correlation of -0.920, compared to a coefficient of correlation of -0.729 for all fields. The range of variation of the hydrographs, i.e., the sensitivity of the runoff response to the soil moisture spatial variability, appeared thus to be minimised in wet conditions. It is worth mentioning that repeated measurements in

Table 3. Runoff peak Q_{max} and total runoff volume V for each antecedent soil moisture scenario for the 10 field campaigns. For the stochastic scenarios, the average Q_{max} and V were computed and the standard deviations are depicted in brackets. Maximum and minimum values for each field campaign are highlighted in bold and italic, respectively.

	Reference	Constant	Structured	Structured$_{inv}$	Random	Variogram	Connected
Walhain – 07/04/2008							
Q_{max} [m^3 h^{-1}]	**250**	153	246	*122*	192 (15)	199 (22)	195 (18)
V [m^3]	5259	4019	**6945**	*3069*	4886 (231)	4896 (353)	4895 (301)
Keispelt – 13/03/2009							
Q_{max} [m^3 h^{-1}]	**529**	*327*	460	334	401 (20)	412 (47)	405 (37)
V [m^3]	6454	3986	**6742**	*3554*	5045 (184)	5138 (563)	5079 (419)
Marbaix – 19/03/2009							
Q_{max} [m^3 h^{-1}]	18	7	**26**	*1*	9 (2)	10 (8)	10 (5)
V [m^3]	150	51	**262**	*4*	66 (18)	81 (68)	71 (41)
Marbaix – 15/04/2009							
Q_{max} [m^3 h^{-1}]	26	10	**29**	*2*	12 (3)	14 (10)	13 (8)
V [m^3]	223	74	**302**	*10*	90 (21)	115 (94)	105 (68)
Walsdorf – 21/07/2009							
Q_{max} [m^3 h^{-1}]	73	*64*	**105**	70	72 (6)	73 (8)	73 (7)
V [m^3]	637	545	**1189**	*513*	653 (58)	659 (77)	658 (66)
Burnia – 15/03/2010							
Q_{max} [m^3 h^{-1}]	**45**	18	43	*15*	25 (4)	31 (16)	28 (11)
V [m^3]	509	142	**739**	*87*	237 (43)	312 (164)	284 (116)
Burnia – 18/03/2010							
Q_{max} [m^3 h^{-1}]	**49**	22	44	*20*	29 (4)	34 (14)	31 (10)
V [m^3]	534	194	**776**	*127*	300 (45)	355 (149)	327 (105)
Burnia – 24/03/2010							
Q_{max} [m^3 h^{-1}]	47	26	**49**	*24*	33 (4)	37 (15)	35 (10)
V [m^3]	494	240	**870**	*154*	349 (46)	407 (160)	391 (114)
Burnia – 30/03/2010							
Q_{max} [m^3 h^{-1}]	240	*112*	**274**	157	195 (16)	250 (52)	230 (41)
V [m^3]	3363	*2025*	**5048**	2170	3172 (128)	3549 (448)	3401 (362)
Burnia – 06/04/2010							
Q_{max} [m^3 h^{-1}]	249	*124*	**283**	158	200 (17)	261 (55)	242 (43)
V [m^3]	3581	2232	**5146**	*2230*	3255 (129)	3654 (504)	3529 (386)

Marbaix and Burnia exhibited a temporal stability of measured soil moisture patterns that may explain the good correlation when considering the fields separately.

The particular behaviour of the *Reference* scenario for Walsdorf, which gave a small runoff peak and volume compared to the other fields, originates from the specific organisation of the measured soil moisture. The wettest part of the field in Walsdorf was observed in the plateau of the field whereas the driest part was located near the outlet, which is highlighted by the negative correlation between the TWI and soil moisture (Table 2, last column). A part of the runoff which was generated in the wettest part may then have reinfiltrated before reaching the outlet.

3.2.2 Hydrographs simulated with the stochastic soil moisture maps

Figure 6 shows the 1000 hydrographs from the *Random* scenario for the field campaign in Marbaix, 15 April 2009. The hydrographs from the four first soil moisture scenarios are also plotted, as well as the average *Random* hydrograph. The 1000 *Random* hydrographs cover a wide range of values but the peak discharge is always lower than the *Reference* and *Structured* hydrographs, denoting the particular arrangements of soil moisture patterns in these scenarios that produced a high discharge, although random simulation could theoretically provide the same soil moisture map as the ones from the *Reference* or *Structured* scenarios.
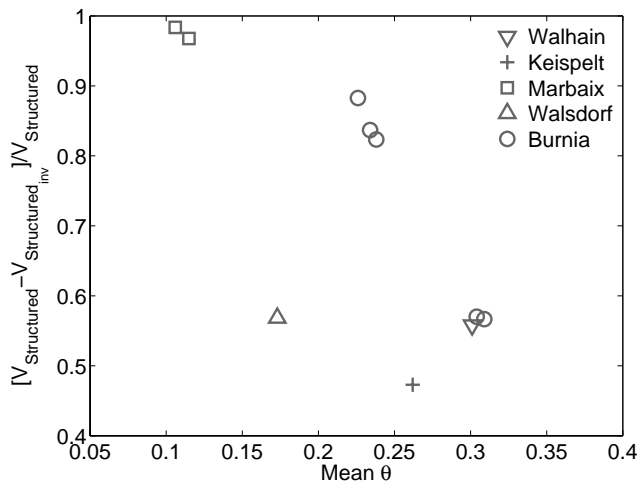
Fig. 5. Relative difference between *Structured* and *Structured*$_{inv}$ runoff volume as a function of the mean soil moisture in the field.
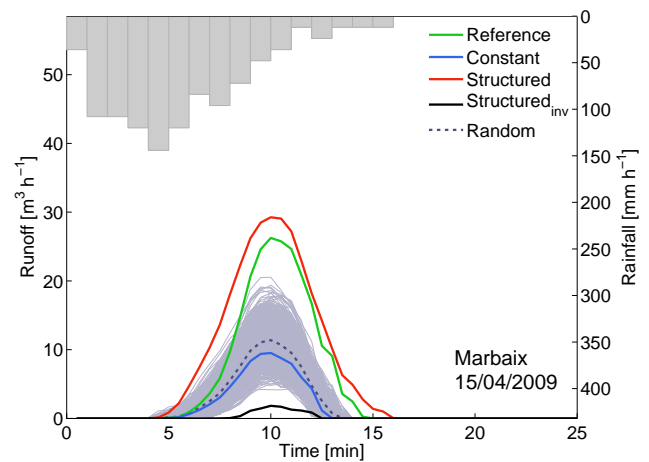

Fig. 6. Hydrographs from hydrologic simulation using the antecedent soil moisture maps from scenarios 1 to 5 for the field campaign in Marbaix, 15 April 2009. The average *Random* hydrograph is depicted as a dotted line on top of the 1000 hydrographs from the random antecedent soil moisture maps.

It is worth noticing that a particular realisation of the *Random* scenario can result in a hydrograph drastically different from another realisation. Other fields than Marbaix, 15 April 2009 showed average *Random* hydrographs that were better approaching the *Reference* one, but there were still a large variability between the realisations.

The hydrographs from the *Variogram* scenario (Fig. 7) cover a wider range of values, largely overlapping the range delineated by the hydrographs from the *Structured* and the *Structured*$_{inv}$ scenarios. The antecedent soil moisture map of the *Variogram* scenario giving the largest discharge was actually characterised by a well-connected soil moisture pattern with the highest soil moisture values near the outlet (map not shown). It was observed that, for all fields, the highest *Variogram* scenario hydrograph showed the largest runoff peak and volume compared to the highest *Random* hydrograph. The hydrographs from the *Connected* scenarios (Fig. 8) also cover a wide range of values, similarly to the *Variogram* coverage. The average hydrographs of the stochastic soil moisture scenarios gave on average higher runoff than the *Constant* scenario.

3.3 Evaluation of soil moisture modelling scenarios

Table 4 shows Nash-Sutcliffe efficiency coefficients (NSE) of the comparison between the different scenarios of antecedent soil moisture maps and the *Reference* scenario, for the ten field campaigns. The comparison of the soil moisture scenarios was performed based on the normalised NSE, that are, the NSE divided by the maximal NSE observed for each field campaign. This normalisation was set such that the mean, the standard deviation and the corresponding statistical tests for each soil moisture scenario can be computed.

The stochastic scenarios of soil moisture, i.e., the *Random*, *Variogram* and *Connected* scenarios performed equally
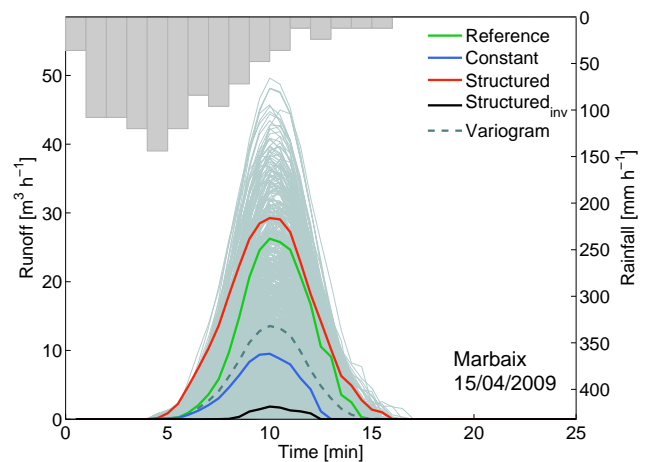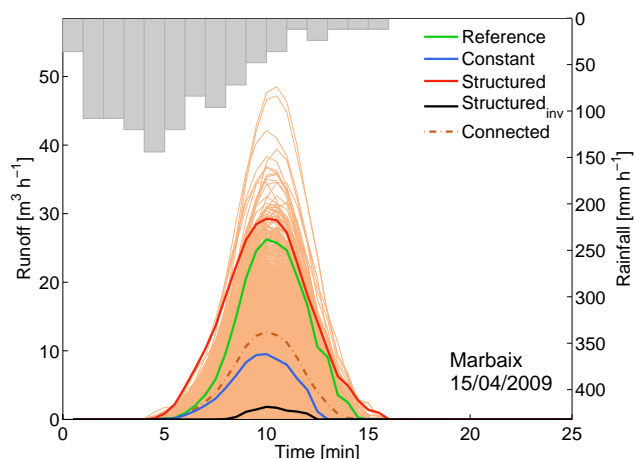

Fig. 7. Hydrographs from hydrologic simulation using the antecedent soil moisture maps from scenarios 1 to 4 and 6 for the field campaign in Marbaix, 15 April 2009. The average *Variogram* hydrograph is depicted in a dashed line on top of the 1000 hydrographs from the simulated antecedent soil moisture maps.

(based on a 95 % confidence interval) and gave on average higher NSE than the deterministic scenarios, especially for the *Variogram* scenario. The *Structured* scenario performed the best among the deterministic scenarios. Neglecting the field campaign of Walsdorf, the averages of the normalised NSE of the *Structured* and the *Constant* scenarios appeared significantly different, with a p-value of 0.0117. Although the *Constant* scenario performed better than the *Structured* one in two field campaigns, i.e., Waldorf and Burnia – 24/03/2010, the *Structured* scenario was found to be a better approach for modelling the soil moisture spatial variability within a catchment than the *Constant* scenario.

Table 4. Nash-Sutcliffe efficiency coefficients of the different scenarios of antecedent soil moisture maps compared to the *Reference* scenario for the 10 field campaigns. The mean and the standard deviation of normalised Nash-Sutcliffe coefficients were computed for the 10 field campaigns. Maximum and minimum values for each field campaign are highlighted in bold and italic, respectively.
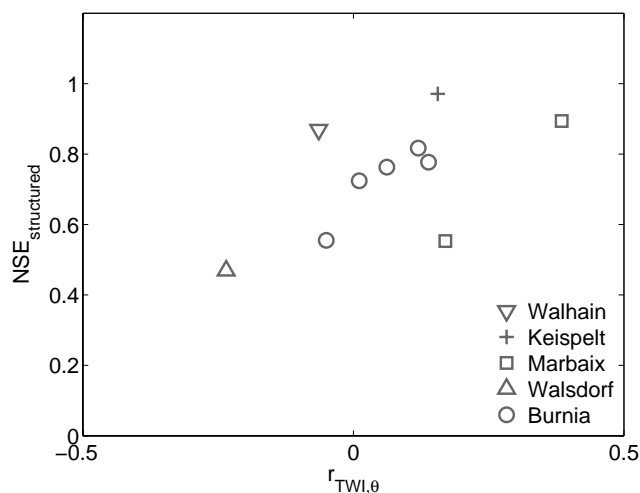
		Constant	Structured	Structured$_{inv}$	Random	Variogram	Connected
Walhain	07/04/2008	0.853	0.869	*0.686*	0.945	**0.946**	0.943
Keispelt	13/03/2009	0.777	**0.971**	*0.650*	0.903	0.911	0.906
Marbaix	19/03/2009	0.513	0.553	*−0.066*	0.646	**0.755**	0.690
Marbaix	15/04/2009	0.491	**0.894**	*−0.030*	0.592	0.719	0.675
Walsdorf	21/07/2009	0.970	*0.469*	0.937	**0.993**	0.991	0.992
Burnia	15/03/2010	0.431	**0.777**	*0.224*	0.672	0.773	0.755
Burnia	18/03/2010	0.551	0.724	*0.378*	0.764	**0.821**	0.792
Burnia	24/03/2010	0.685	0.555	*0.506*	0.863	**0.903**	0.896
Burnia	30/03/2010	*0.666*	0.763	0.837	0.889	**0.920**	0.915
Burnia	06/04/2010	*0.688*	0.817	0.808	0.887	**0.922**	0.910
Mean*		0.736	0.834	0.531	0.913	0.974	0.951
Standard deviation*		0.136	0.178	0.374	0.101	0.062	0.075

* The mean and standard deviation were computed based on normalised Nash-Sutcliffe coefficients.

Fig. 8. Hydrographs from hydrologic simulation using the antecedent soil moisture maps from scenarios 1 to 4 and 7 for the field campaign in Marbaix, 15 April 2009. The average *Connected* hydrograph is depicted in a dashed-dotted line on top of the 1000 hydrographs from the simulated antecedent soil moisture maps.

Fig. 9. Nash-Sutcliffe efficiency coefficients of the *Structured* scenario with respect to the *Reference* scenario (NSE$_{structured}$) as a function of the correlation between measured soil moisture and the TWI ($r_{TWI,\theta}$).

Figure 9 presents the NSE of the *Structured* scenario with respect to the *Reference*, as a function of the correlation between measured soil moisture and the TWI. The performance of the *Structured* scenario in approaching the *Reference* hydrograph (i.e., NSE$_{structured}$) appeared to be related to the explanatory power of the TWI for soil moisture (i.e., $r_{TWI,\theta}$), with a coefficient of correlation of 0.581 between these two variables. This correlation increased if we consider only field campaigns performed on the same field, e.g., the correlation rose to 0.898 when field acquisitions in Burnia only were considered. The bad performance of the *Structured* scenario in approaching the *Reference* scenario for Walsdorf pointed

out above can be related to its negative correlation between the TWI and measured soil moisture. Similarly, the proximity of the *Reference* and *Structured* hydrographs for Marbaix – 15/04/2009 (Fig. 4b) can be related to the largest correlation between the TWI and soil moisture that was observed for this campaign.

Varying grid sizes did not drastically change the hydrographs that were obtained with the 10 m resolution simulations (see Fig. 4b). While the correlation between TWI and measured soil moisture slightly increased with grid size, there was not a clear increase of the NSE for the *Structured* scenario (Table 5).

Table 5. Nash-Sutcliffe efficiency coefficients of the different scenarios of antecedent soil moisture maps compared to the *Reference* scenario for Marbaix, 15 April 2010 for varying grid sizes. The coefficients of correlation between the TWI and soil moisture ($r_{\mathrm{TWI},\theta}$) are presented in the second column.

Grid size	$r_{\mathrm{TWI},\theta}$	Constant	Structured	Structured$_{\mathrm{inv}}$	Random	Variogram	Connected
10 m	0.385	0.491	0.894	−0.030	0.592	0.719	0.675
12.5 m	0.383	0.611	0.914	0.185	0.689	0.770	0.708
15 m	0.387	0.378	0.913	−0.097	0.485	0.542	0.522
17.5 m	0.427	0.660	0.973	0.294	0.724	0.793	0.748
20 m	0.488	0.550	0.989	0.235	0.618	0.676	0.641
22.5 m	0.393	0.421	0.798	−0.098	0.485	0.551	0.509
25 m	0.488	0.557	0.899	0.219	0.599	0.637	0.613
27.5 m	0.439	0.531	0.945	0.169	0.591	0.608	0.599
30 m	0.668	0.693	0.898	−0.001	0.788	0.815	0.805

4 Discussions

4.1 Effect of spatial variability of soil moisture on simulated runoff

Hydrologic simulations using different organisations of soil moisture patterns showed a large variability of runoff responses. This behaviour can be explained by the location of the runoff contributing and non-contributing (or even reinfiltrating) areas that are determined by antecedent soil moisture conditions (Noto et al., 2008). Runoff is generated at a certain soil moisture threshold because rainfall intensity exceeds the effective infiltration capacity (Hortonian overland flow). Based on single-cell hydrologic simulation, the antecedent soil moisture thresholds that triggered runoff generation were estimated to be approximately 0.25 and 0.20 m^3 m^{-3} for the 25 and 20 mm h^{-1} initial hydraulic conductivity, respectively. The threshold behaviour of the hydrologic model response to antecedent soil moisture results in a non-linear response of the model with soil moisture. Introducing spatial variability of soil moisture creates zones where the initial soil moisture is close or above this threshold, which rapidly become runoff contributing areas. The runoff response of the different soil moisture scenarios can be explained by the locations of runoff contributing areas that modulated the simulated runoff response at the catchment outlet:

– The *Constant* scenario resulted in smaller runoff than other spatially variable soil moisture scenarios (except the *Structured*$_{\mathrm{inv}}$), denoting the non-linear response of the hydrologic model to soil moisture. Merz and Plate (1997); Merz and Bardossy (1998) and Bronstert and Bardossy (1999) also observed that constant soil moisture conditions resulted in the lowest discharge compared to spatially-variable soil moisture, either organised in a structured (Merz and Plate, 1997; Merz and Bardossy, 1998; Bronstert and Bardossy, 1999) or random (Merz and Bardossy, 1998; Bronstert and Bardossy, 1999) way. However, compared to spatially-constant soil moisture organisation, Merz and Plate (1997) observed similar (dry conditions) and smaller (wet conditions) discharge with randomly permuted values. This was explained by the possibility of re-infiltrating pixels placed along the flow channel, but this explanation was incoherent when comparing the results in dry and wet conditions. In our case, although some random realisations resulted in smaller discharge than the *Constant* scenarios, the average *Random* hydrographs appeared larger than the *Constant* ones, maybe due to the larger number of realisations in our study (1000 instead of 3) or to the different model parameterisations.

– The *Structured* scenario gave the largest discharge due to the locations of the contributing areas (i.e., the wettest areas) that were situated near the outlet and in the flow channels. However, for the *Structured*$_{\mathrm{inv}}$ scenario, the contributing areas were far from the outlet and from the runoff network, so the generated runoff re-infiltrated when propagated to the field outlet.

– The decrease in the range of hydrographs, expressed as the difference between the *Structured* and *Structured*$_{\mathrm{inv}}$ scenarios, with increasing mean soil moisture (Fig. 5) can be explained by the increasing size of the contributing areas in wet conditions. In dry conditions, small contributing areas are located near to and far from the outlet for the *Structured* and the *Structured*$_{\mathrm{inv}}$ scenarios, respectively. As a result, the difference between these scenarios is maximised in dry conditions. Therefore, field acquisitions (i.e., Marbaix, Walsdorf and the first three dates of Burnia) that showed antecedent soil moisture below the soil moisture thresholds are expected to be more sensitive to spatial variability of soil moisture as thresholds are overtaken during the simulations. In wet conditions, the contributing areas expand and tend to cover the whole field, and as a result, the difference between the two scenarios tends to vanish. At an

extreme state of wetness, i.e., for a completely saturated soil, there would be no differences in terms of runoff between the two extreme scenarios. In that respect, Merz and Plate (1997) also pointed out that the effect of simulated spatially structured variability was more important in dry conditions because of the smaller size of the contributing areas.

– The average *Random*, *Variogram* or *Connected* hydrographs (i.e., the model outputs) appeared larger from the *Constant* hydrograph, although the average *Random*, *Variogram* or *Connected* antecedent soil moisture maps (i.e., the model inputs) are theoretically equals to the *Constant* one, denoting the non-linearity of the hydrologic model.

– The *Variogram* and *Connected* soil moisture scenarios gave a wider range of hydrographs and on average higher runoff peak and volume compared to the *Random* soil moisture scenario because of the spatial coherence of contributing areas, as it was also stated in Merz and Bardossy (1998). This wide range is to be attributed to the spatial clustering of non-contributing reinfiltrating pixels that can be placed on or completely outside the flow channel, resulting in a small or great discharge, respectively. The probability that numerous reinfiltrating pixels are present on the flow channel is smaller in the *Random* scenario than in the *Variogram* and *Connected* scenarios because of the grouping of similar pixels.

– It was shown that a unique realisation of the *Random* scenario can not be used to properly model soil moisture patterns because of the large variability in modelled discharges. From a practical point of view, the *Random* scenario may suffer from the large requirement in computing resources, due to the need of several repetitions. This large variability between the realisations with the *Random* scenario compared to a structured soil moisture organisation was not observed in Merz and Plate (1997) and Merz and Bardossy (1998). It seems that the threshold effect of soil moisture on runoff was stronger in our study than in these two previous ones, allowing for more re-infiltration and a larger impact of the locations of the contributing areas.

The second objective of this paper was to evaluate which description of soil moisture organisation is the most appropriate for hydrologic modelling at the field scale. The comparability of the fields may be limited by soil, topographic, resolution and moisture conditions differences. Nevertheless, the good performance of the *Structured* soil moisture scenario was observed for different field and moisture conditions, even in cases when measured soil moisture was poorly correlated with the TWI. It was shown that there was a larger comparability between the different soil moisture conditions for field campaigns performed on same fields (Burnia and

Marbaix), even though there was a large variability of the runoff peak and volume amounts depending on the wetness conditions. Varying grid sizes did not alter the order of performance of the antecedent soil moisture scenarios (Table 5). It was thus shown that, to some extent, the effect of spatial variability of antecedent soil moisture can be observed in various field conditions at the field scale, under a specific rainfall.

4.2 Soil moisture patterns and its relation with topographic wetness index

In this study, the TWI appeared to be a poor predictor of the measured soil moisture spatial distribution (see Table 2). Although some studies have shown that the explanatory power of the TWI for soil moisture may increase with scale aggregation (Sørensen et al., 2006) or by comparing grid cells accounting for an uncertainty in the location of the cells (Güntner et al., 2004), this was only slightly observed when increasing the resolution scale (i.e., for Marbaix, 15 April 2009 only). Meanwhile, the use of multidirectional flow accumulation algorithms could also improve the computation of the TWI and its correlation with measured soil moisture (Quinn et al., 1995; Tarboton, 1997; Seibert and McGlynn, 2007). The explanatory power of the TWI for soil moisture may be limited in dry conditions, as observed for Walsdorf. Indeed, for this case, the soil moisture pattern may be better explained by soil type or radiative indices, as it was the only field campaign that was conducted in summer.

The predictive power of the *Structured* scenario appeared to be related to the correlation between the measured soil moisture and the TWI (Fig. 9). Nevertheless, for some field campaigns, this weak negative correlation contrasted with the rather good NSE of the *Reference* scenario compared to the *Structured* scenario, as for, e.g., Walhain, 7 April 2008, which has $r_{\text{TWI},\theta} = -0.064$ and $\text{NSE}_{\text{structured}} = 0.869$. This can be explained by the non-unicity of the hydrologic model with respect to the antecedent soil moisture maps for a particular hydrograph, that is, a large number of antecedent soil moisture maps can result in the same hydrograph. In that respect, a measured soil moisture pattern which is poorly correlated with the TWI could still result in a runoff response close to the one of the *Structured* scenario.

In the hydrologic simulations using CREHDYS, flow paths are governed by topography, but it is worth noticing that in reality, deviating structure within (e.g., wheel tracks) and between (e.g., ditches, roads) fields may limit the use of solely topographically-driven hydrologic modelling. If not accounted for in real case experiment, it would reduce the relationship between the explanatory power of the TWI for soil moisture and the runoff response using the *Structured* scenario. In these simulations, the same topography information (e.g., same grid resolution) is used for both hydrological modelling and reordering soil moisture in the *Structured*

scenario. This might have increased the correlation between the NSE$_{structured}$ and the explanatory power of the TWI for measured soil moisture.

Grayson et al. (1997) showed that soil moisture patterns tend to be characterised by a larger stochastic variability in dry conditions while they appear more structured in wet conditions. Nevertheless, for the 10 soil moisture datasets presented here, there was no clear trend between the mean soil moisture and the importance of the nugget effect (Table 2), except for Burnia where a decrease in the Nugget/Sill ratio is observed with increasing soil moisture. The overall poor relation may originate from the different field conditions in terms of soil type and topography and from the limited soil moisture range of the field campaigns.

4.3 Disaggregation of soil moisture

Disaggregating coarse-scale soil moisture data into fine-scale patterns needs to account for the importance of spatial variability on runoff responses. For large catchments (>10 km), spatial distribution of soil moisture can not be measured at high resolution (e.g., $\sim$m) at the field scale. Nevertheless, coarse-scale remotely-sensed soil moisture data could be disaggregated by combining a geostatistical description of fine-scale soil moisture patterns with other sources of fine-scale information (e.g., topography as in Pellenq et al., 2003), if soil moisture patterns could be explained by this information. In that respect, several authors have proposed empirical relationships between the mean soil moisture and its corresponding standard deviation for different extent scales using soil moisture data from remote sensing estimates and invasive sensors at various extent scales (Western et al., 2003; Vereecken et al., 2007; Famiglietti et al., 2008). Therefore, fine-scale antecedent soil moisture maps are to be modeled from coarse-scale remotely-sensed soil moisture data according to the effects of soil moisture spatial variability on runoff response.

5 Conclusions

We investigated the effect of antecedent soil moisture spatial variability on runoff response using a distributed hydrologic model at the field scale. Ten field acquisitions of soil moisture at high resolution were obtained using a mobile proximal GPR platform. Based on these soil moisture data, seven scenarios of antecedent soil moisture maps were constructed with different spatial organisations. Hydrologic simulations were then performed for each field acquisition with seven antecedent soil moisture scenarios.

The first objective of this study was to investigate the effect of different antecedent soil moisture scenarios on field scale runoff response. The high sensitivity of antecedent soil moisture spatial variability on the runoff response was clearly

shown for all the field acquisitions in various field and moisture conditions, but in a larger extent in dry conditions. Spatially constant antecedent soil moisture conditions (*Constant* scenario) resulted in a smaller discharge than scenarios exhibiting soil moisture spatial variability, except for the *Structured*$_{inv}$ scenario. When soil moisture was arranged according to the TWI (*Structured* scenario), the runoff volume was the largest for all field campaigns. At the opposite, when soil moisture was inversely arranged according to the TWI (*Structured*$_{inv}$ scenario), the runoff volume was in general the lowest. Stochastic scenarios of antecedent soil moisture (i.e., *Random*, *Variogram* and *Connected*) gave on average similar and intermediate hydrographs, but there was a wide variability between the stochastic realisations. The observed effects of soil moisture spatial variability on the runoff could be explained in terms of contributing areas, with respect to their sizes and their locations within the field, as runoff is triggered above a soil moisture threshold. The spatial variability of antecedent soil moisture conditions therefore resulted in different runoff responses compared to field-averaged values because of the non-linearity of the runoff production to antecedent soil moisture.

The second objective of this study was to find the soil moisture scenarios that most closely approach the measured soil moisture pattern in terms of runoff response. The average hydrograph from the *Variogram* scenario was the best soil moisture modelling scenario. Yet, it is worth noting that a particular realisation can perform very badly. Among the deterministic soil moisture scenarios, *Structured* performed the best, which was moderately related to the correlation of measured soil moisture and the TWI itself.

Except few particular cases, the effects of spatial variability of soil moisture on runoff response which were already analysed in previous studies (Merz and Plate, 1997; Merz and Bardossy, 1998; Bronstert and Bardossy, 1999) could be generalised for various field and moisture conditions. In the absence of other detailed source of information, organising the soil moisture pattern accordingly to the TWI appeared to be the best soil moisture modelling method, even when TWI was poorly correlated to measured soil moisture. Given the high availability of topographic data at high resolution, disaggregating remotely-sensed soil moisture data using TWI information might be valuable. Nevertheless, these findings may be better validated against real discharge measurements.

Edited by: J. Seibert

References

Beven, K. J. and Kirkby, M. J.: A physically based, variable contributing area model of basin hydrology, Hydrological Sciences Bulletin, 24, 43–69, 1979.

Blöschl, G. and Sivapalan, M.: Scale Issues in Hydrological Modeling – A Review, Hydrol. Process., 9, 251–290, 1995.

Brocca, L., Melone, F., Moramarco, T., Wagner, W., Naeimi, V., Bartalis, Z., and Hasenauer, S.: Improving runoff prediction through the assimilation of the ASCAT soil moisture product, Hydrol. Earth Syst. Sci., 14, 1881–1893, doi:10.5194/hess-14-1881-2010, 2010.

Bronstert, A. and Bárdossy, A.: The role of spatial variability of soil moisture for modelling surface runoff generation at the small catchment scale, Hydrol. Earth Syst. Sci., 3, 505–516, doi:10.5194/hess-3-505-1999, 1999.

Capehart, W. J. and Carlson, T. N.: Decoupling of surface and near-surface soil water content: A remote sensing perspective, Water Resour. Res., 33, 1383–1395, 1997.

Castillo, V. M., Gomez-Plaza, A., and Martinez-Mena, M.: The role of antecedent soil water content in the runoff response of semi-arid catchments: a simulation approach, J. Hydrol., 284, 114–130, 2003.

Crow, W. T. and Ryu, D.: A new data assimilation approach for improving runoff prediction using remotely-sensed soil moisture retrievals, Hydrol. Earth Syst. Sci., 13, 1–16, doi:10.5194/hess-13-1-2009, 2009.

Crow, W. T., Wood, E. F., and Dubayah, R.: Potential for downscaling soil moisture maps derived from spaceborne imaging radar data, J. Geophys. Res.-Atmos., 105, 2203–2212, 2000.

Famiglietti, J. S., Ryu, D., Berg, A. A., Rodell, M., and Jackson, T. J.: Field observations of soil moisture variability across scales, Water Resour. Res., 44, W01423, doi:10.1029/2006WR005804, 2008.

Gütner, A., Seibert, J., and Uhlenbrook, S.: Modeling spatial patterns of saturated areas: An evaluation of different terrain indices, Water Resour. Res., 40, W05114, doi:10.1029/2003WR002864, 2004.

Grayson, R. B., Western, A. W., Chiew, F. H. S., and Blöschl, G.: Preferred states in spatial soil moisture patterns: Local and non-local controls, Water Resour. Res., 33, 2897–2908, 1997.

Green, W. and Ampt, G.: Studies on soil physics: 1, flow of air and water through soils, J. Agr. Sci., 4, 1–24, 1911.

Houser, P. R., Shuttleworth, W. J., Famiglietti, J. S., Gupta, H. V., Syed, K. H., and Goodrich, D. C.: Integration of soil moisture remote sensing and hydrologic modeling using data assimilation, Water Resour. Res., 34, 3405–3420, 1998.

Huisman, J. A., Hubbard, S. S., Redman, J. D., and Annan, A. P.: Measuring soil water content with ground penetrating radar: A review, Vadose Zone J., 2, 476–491, 2003.

Jadoon, K. Z., Lambot, S., Scharnagl, B., van der Kruk, J., Slob, E., and Vereecken, H.: Quantifying field-scale surface soil water content from proximal GPR signal inversion in the time domain, Near Surf. Geophys., 8, 483–491, doi:10.3997/1873-0604.2010036, 2010.

Kuo, W. L., Steenhuis, T. S., McCulloch, C. E., Mohler, C. L., Weinstein, D. A., DeGloria, S. D., and Swaney, D. P.: Effect of grid size on runoff and soil moisture for a variable-source-area hydrology model, Water Resour. Res., 35, 3419–3428, 1999.

Laloy, E. and Bielders, C. L.: Plot scale continuous modelling of runoff in a maize cropping system with dynamic soil, surface properties, J. Hydrol., 349, 455–469, 2008.

Laloy, E. and Bielders, C. L.: Modelling intercrop management impact on runoff and erosion in a continuous maize cropping system: Part I. Model description, global sensitivity analysis and Bayesian estimation of parameter identifiability, Eur. J. Soil Sci., 60, 1005–1021, 2009.

Laloy, E., Fasbender, D., and Bielders, C. L.: Parameter optimization and uncertainty analysis for plot-scale continuous modeling of runoff using a formal Bayesian approach, J. Hydrol., 380, 82–93, 2010.

Lambot, S., Slob, E. C., van den Bosch, I., Stockbroeckx, B., and Vanclooster, M.: Modeling of ground-penetrating radar for accurate characterization of subsurface electric properties, IEEE Trans. Geosci. Remote Sensing, 42, 2555–2568, 2004.

Lambot, S., Weihermüller, L., Huisman, J. A., Vereecken, H., Vanclooster, M., and Slob, E. C.: Analysis of air-launched ground-penetrating radar techniques to measure the soil surface water content, Water Resour. Res., 42, W11403, doi:10.1029/2006WR005097, 2006.

Lambot, S., Binley, A., Slob, E. C., and Hubbard, S.: Ground penetrating radar in hydrogeophysics, Vadose Zone J., 7, 137–139, 2008a.

Lambot, S., Slob, E. C., Chavarro, D., Lubczynski, M., and Vereecken, H.: Measuring soil surface water content in irrigated areas of southern Tunisia using full-waveform inversion of proximal GPR data, Near Surf. Geophys., 6, 403–410, 2008b.

Loew, A. and Mauser, W.: On the disaggregation of passive microwave soil moisture data using a priori knowledge of temporally persistent soil moisture fields, IEEE Trans. Geosci. Remote Sensing, 46, 819–834, doi:10.1109/TGRS.2007.914800, 2008.

Marquardt, D. W.: An algorithm for least-squares estimation of nonlinear parameters, J. Soc. Indust. Appl. Math., 11, 431–441, 1963.

Merlin, O., Chehbouni, A., Boulet, G., and Kerr, Y.: Assimilation of disaggregated microwave soil moisture into a hydrologic model using coarse-scale meteorological data, J. Hydrometeorol., 7, 1308–1322, 2006.

Merz, B. and Bardossy, A.: Effect of spatial variability on the rainfall runoff process in a small loess catchment, J. Hydrol., 212, 304–317, 1998.

Merz, B. and Plate, E. J.: An analysis of the effects of spatial variability of soil and soil moisture on runoff, Water Resour. Res., 33, 2909–2922, 1997.

Minet, J., Lambot, S., Slob, E., and Vanclooster, M.: Soil surface water content estimation by full-waveform GPR signal inversion in the presence of thin layers, IEEE Trans. Geosci. Remote Sensing, 48, 1138–1150, doi:10.1109/TGRS.2009.2031907, 2010.

Minet, J., Wahyudi, A., Bogaert, P., Vanclooster, M., and Lambot, S.: Mapping shallow soil moisture profiles at the field scale using full-waveform inversion of ground penetrating radar data, Geoderma, 161, 225–237, doi:10.1016/j.geoderma.2010.12.023, 2011.

Noto, L. V., Ivanov, V. Y., Bras, R. L., and Vivoni, E. R.: Effects of initialization on response of a fully-distributed hydrologic model, J. Hydrol., 352, 107–125, 2008.

Pauwels, V. R. N., Hoeben, R., Verhoest, N. E. C., and De Troch, F. P.: The importance of the spatial patterns of remotely sensed soil moisture in the improvement of discharge predictions for

small-scale basins through data assimilation, J. Hydrol., 251, 88–102, 2001.

Pellenq, J., Kalma, J., Boulet, G., Saulnier, G., Wooldridge, S., Kerr, Y., and Chehbouni, A.: A disaggregation scheme for soil moisture based on topography and soil depth, J. Hydrol., 276, 112–127, doi:10.1016/S0022-1694(03)00066-0, 2003.

Quinn, P. F., Beven, K. J., and Lamb, R.: The LN(A/tan-BETA) index - How to calculate it and how to use it within the TOP-MODEL framework, Hydrol. Process., 9, 161–182, 1995.

Rhoades, J. D., Raats, P. A. C., and Prather, R. J.: Effects of liquid-phase electrical conductivity, water content, and surface conductivity on bulk soil electrical conductivity, Soil Sci. Soc. Am. J., 40, 651–655, 1976.

Robinson, D. A., Campbell, C. S., Hopmans, J. W., Hornbuckle, B. K., Jones, S. B., Knight, R., Ogden, F., Selker, J., and Wendroth, O.: Soil moisture measurement for ecological and hydrological watershed-scale observatories: A review, Vadose Zone J., 7, 358–389, 2008.

Savabi, M. and Williams, J.: Water balance and percolation. In: Flanagan, D.C., Nearing, M.A. (Eds.), USDA – Water Erosion Prediction Project: Hillslope profile model documentation (Chapter 5). Nserl report no. 2., Tech. rep., USDA-ARS National Soil Erosion Research Laboratory, West Lafayette, Indiana, 1995.

Seibert, J. and McGlynn, B. L.: A new triangular multiple flow direction algorithm for computing upslope areas from gridded digital elevation models, Water Resour. Res., 43, W04501, doi:10.1029/2006WR005128, 2007.

Serbin, G. and Or, D.: Ground-penetrating radar measurement of crop and surface water content dynamics, Remote Sens. Environ., 96, 119–134, 2005.

Sørensen, R., Zinko, U., and Seibert, J.: On the calculation of the topographic wetness index: evaluation of different methods based on field observations, Hydrol. Earth Syst. Sci., 10, 101–112, doi:10.5194/hess-10-101-2006, 2006.

Tarboton, D.: A new method for the determination of flow directions and upslope areas in grid digital elevation models, Water Resour. Res., 33, 309–319, 1997.

Topp, G. C., Davis, J. L., and Annan, A. P.: Electromagnetic Determination of Soil Water Content: Measurements in Coaxial Transmission Lines, Water Resour. Res., 16, 574–582, 1980.

Van Orshoven, J. and Vandenbroucke, D.: Guide de l'utilisateur d'AARDEWERK, base de données pédologiques, Institute for land and water management, K.U. Leuven, Leuven, Belgium, Tech. rep., 1993.

Vereecken, H., Kamai, T., Harter, T., Kasteel, R., Hopmans, J., and Vanderborght, J.: Explaining soil moisture variability as a function of mean soil moisture: a stochastic unsaturated flow perspective, Geophys. Res. Lett., 34, L22402, doi:10.1029/2007GL031813, 2007.

Vereecken, H., Huisman, J. A., Bogena, H., Vanderborght, J., Vrugt, J. A., and Hopmans, J. W.: On the value of soil moisture measurements in vadose zone hydrology: A review, Water Resour. Res., 44, W00D06, doi:10.1029/2008WR006829, 2008.

Wagner, W., Blöschl, G., Pampaloni, P., Calvet, J. C., Bizzarri, B., Wigneron, J. P., and Kerr, Y.: Operational readiness of microwave remote sensing of soil moisture for hydrologic applications, Nord. Hydrol., 38, 1–20, 2007.

Weihermüller, L., Huisman, J. A., Lambot, S., Herbst, M., and Vereecken, H.: Mapping the spatial variation of soil water content at the field scale with different ground penetrating radar techniques, J. Hydrol., 340, 205–216, 2007.

Western, A., Grayson, R., Blöschl, G., and Wilson, D.: Spatial Variability of Soil Moisture and Its Implications for scaling, chap. 8, 119–142, CRC PRESS, 2003.

Western, A. W., Grayson, R. B., Blöschl, G., Willgoose, G. R., and McMahon, T. A.: Observed spatial organization of soil moisture and its relation to terrain indices, Water Resour. Res., 35, 797–810, 1999.

Zehe, E. and Blöschl, G.: Predictability of hydrologic response at the plot and catchment scales: Role of initial conditions, Water Resour. Res., 40, W10202, doi:10.1029/2003WR002869, 2004.

Zehe, E., Becker, R., Bardossy, A., and Plate, E.: Uncertainty of simulated catchment runoff response in the presence of threshold processes: Role of initial soil moisture and precipitation, J. Hydrol., 315, 183–202, 2005.

Zehe, E., Graeff, T., Morgner, M., Bauer, A., and Bronstert, A.: Plot and field scale soil moisture dynamics and subsurface wetness control on runoff generation in a headwater in the Ore Mountains, Hydrol. Earth Syst. Sci., 14, 873–889, doi:10.5194/hess-14-873-2010, 2010.

Zinn, B. and Harvey, C. F.: When good statistical models of aquifer heterogeneity go bad: A comparison of flow, dispersion, and mass transfer in connected and multivariate Gaussian hydraulic conductivity fields, Water Resour. Res., 39, 1051, doi:10.1029/2001WR001146, 2003.